MHD pressure drop estimate for the WCLL in-magnet PbLi loop

Alessandro Tassone[1]*, Simone Siriano[1], Gianfranco Caruso[1], Marco Utili[2], Alessandro Del Nevo[2]

[1] *DIAEE Nuclear Section - Sapienza University of Rome, Corso Vittorio Emanuele II, 244, 00186, Roma, Italy*

[2] *ENEA FSN-ING-PAN, ENEA CR Brasimone, 40032, Camugnano (BO), Italy*

Abstract

In the Water-Cooled Lithium Lead (WCLL) blanket, the eutectic alloy lithium-lead (PbLi) is used as tritium breeder and carrier, neutron multiplier, and heat transfer medium. The PbLi hydraulic loop section in the range of the reactor field coils, which includes the blanket and a non-negligible length of the connection pipes, is affected by intense magnetic fields which cause the transition to a MHD regime. Lorentz forces oppose the fluid motion and cause pressure losses several orders of magnitude higher than for the ordinary hydrodynamic regime. An accurate estimate of the MHD pressure drop is mandatory to properly design the PbLi loop and to optimize the flow path in the blanket. In this paper, the so-called "in-magnet" section of the PbLi loop is divided into three main regions (feeding and draining pipe, manifold, and breeding zone) which are further discretized into basic hydraulic elements. Analytical correlations and numerical results available in the literature are then used to calculate the MHD pressure drop terms for each element and then the overall loss. The study highlights that the highest contribution to pressure loss is made by the spinal manifold and connection pipes. Optimization strategies are suggested to minimize losses in these elements.

Keywords: Magnetohydrodynamics (MHD), WCLL, blanket engineering, DEMO reactor, PbLi, pressure drop

1. Introduction

In the Water-Cooled Lithium Lead (WCLL) blanket concept, the Lithium Lead eutectic alloy (PbLi) fulfills the functions of tritium breeder, carrier, and neutron multiplier, whereas cooling and power extraction is delegated to pressurized water. This solution allows to minimize PbLi velocity and reduce the impact of magnetohydrodynamic (MHD) issues, like electromagnetic pressure losses and enhanced corrosion rates, on the component performances. Nevertheless, these phenomena maintain a significant influence on the blanket layout and, therefore, their quantification and understanding is required to improve and optimize the blanket design [1–3].

In this paper, the attention is focused on the MHD loss in the PbLi loop section which is subjected to a significant magnetic field (> 0.1 T), which is referred as the "in-magnet" PbLi loop. The problem is studied from a component engineering perspective and, combining correlations and numerical results available in literature, is possible to derive a first rough figure that can be used to guide the loop design and highlight critical regions. Due to the wide scope and computational tool limitations, a system-level approach is used that, even if somehow lacking in detail, allows to focus on the main phenomena and progressively iterate toward a more accurate estimate.

A similar methodology was first used by Reimann et al. to assess the importance of MHD loss and other effects in Dual-Coolant and Water-Cooled blankets [4]. More recently, analyses of pressure loss at blanket level has been performed for the Dual-Coolant Lithium Lead [5] and, by means of direct numerical simulation, for the Indian Lithium Lead cooled Ceramic Blanket [6]. Regarding the WCLL, an in-depth comparative analysis on the blanket and breeder circuit layout influence on MHD loss was realized in 2018 to select the most promising configuration for further development [7]. This study aims to update the OB analysis, presented in Ref. [7], to the most recent blanket design and, furthermore, to extend it by including the inboard loop that, until recently, did not possess a sufficient design maturity.

2. WCLL blanket geometry

The blanket completely surrounds the vacuum chamber and is divided into 16 sectors, each one approximately covering a 22.5° toroidal arc. This sector is further divided into 2 and 3 segments, respectively composing the inboard (IB) and outboard (OB) section. The individual segment is composed by a single monolithic module (often labeled "banana"). A radial depth of ≈ 1 m is allotted to the blanket, which weight is sustained by the vacuum vessel (VV) through the Back Supporting Structure (BSS). Plasma containment is ensured by low temperature superconducting Nb_3Sn magnets: 1 Central Solenoid, 16 Toroidal Field Coils (TFC), and 6 Poloidal Field Coils (PFC) [2].

*Corresponding author: alessandro.tassone@uniroma1.it

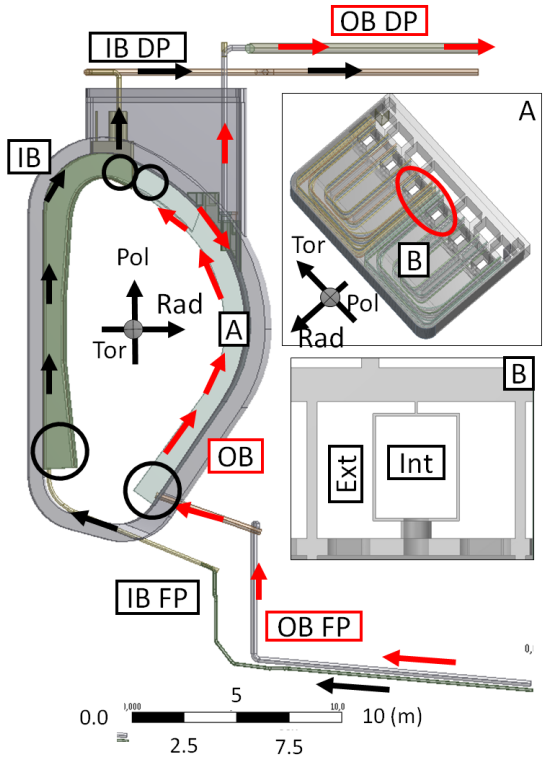

Figure 1: WCLL IB/OB PbLi loop system. The PbLi hydraulic path in the IB and OB is marked with arrows. The position of terminal collectors is highlighted with circles. Detail A: position of spinal manifold in OB toroidal-radial cross-section. Detail B: OB spinal manifold with co-axial rectangular channels, toroidal-radial cross-section.

The PbLi loop system, shown in Fig. 1, is divided into two branches dedicated to feed either one IB or OB segment and circulated by mechanical pumps, which are selected over electromagnetic or permanent magnet pumps thanks to their higher efficiency [3]. Every segment is independently loaded and unloaded by two connection elements, the feeding (FP) and draining pipe (DP), that link blanket and PbLi loop. Consequently, only a modest part of the loop length is subjected to a substantial (> 0.1 T) magnetic field. It is within this region, i.e. the "in-magnet" PbLi loop, where MHD losses start to become relevant and, in particular, the section enclosed by TFC, i.e. "in-vessel" loop, is the most critical.

It is challenging to define exactly the in-magnet loop boundaries since the PFC field can extend quite far inside the tokamak building. In this work, we assume that the magnetic field intensity is negligible in the volume for which $R > 24$ m and $|Z| > 14$ m. The region of interest is then divided into connection pipes, consisting of the FP and DP, and the blanket. The blanket is further broken down into three separate hydraulic regions: terminal collector, spinal manifold, and breeding zone.

Inboard and outboard FP are routed through the VV lower port, whereas DPs are placed in the upper port. Although the former components share a similar layout,

Table 1: Poloidal field in T for PbLi loop hydraulic regions [7]

	Inboard	Outboard
Feeding pipe	0.53 - 1.41	0.53 - 2.96
Bottom collector	0.56	0.80
Top collector	0.41	0.42
Draining pipe	0.29 - 1.26	0.33 - 0.8

DPs differ for their attachment positions with IB DP being at the segment top, while the OB DP is located at ≈2/3 blanket height and requires an additional spinal collector, which is embedded in the BSS. Intermediate manifolds receive the flow incoming from OB sector DPs to reduce encumbrance in the upper port.

A modular geometry is adopted for the OB breeding zone that is divided into an elementary cell by toroidal-radial and radial-poloidal stiffening plates (SP) within which PbLi follows a quasi-radial flow path and is cooled by radial-toroidal-radial cooling pipes. Breeder velocity in this region is about 0.2 mm s^{-1} for the OB and, therefore, its contribution to MHD losses is negligible [7]. PbLi distribution and retrieval is accomplished through a spinal manifold composed of two co-axial rectangular channels. Collectors are located at segment extremities to connect manifold and FP/DP.

3. Methodology

The most recent baseline data is used to derive the accurate magnetic field intensity in the region of interest [7]. The DEMO magnetic field is composed of two components, toroidal and poloidal. The toroidal field is the highest and its intensity at an arbitrary radial coordinate ($B(R)$) is described by the relation

$$B(R)/B_0 = R_0/R \tag{1}$$

where $R_0 = 8.9316$ m and $B_0 = 4.8935$ T. This relation is strictly valid only in the region encompassed by the internal TFC surface, whereas outside of the external TFC surface is null. A region of fringing field, characterized by strong gradients, is found within TFC thickness. Typical field intensities range from 3.35 to 5.20 T (OB) and 5.20 to 8.64 T (IB). Poloidal field is generated by PFC interaction and, being weaker than the toroidal one, exerts a significant effect only for toroidally aligned flow in the terminal collectors and connection pipes. An overview of poloidal field values is collected in Table 1.

The PbLi loop is assumed isothermal at $T_{\text{ref}} = 600$ K with PbLi and Eurofer physical properties evaluated from correlations available in Refs. [8, 9]. PbLi heating over this temperature may happen in the actual blanket, but it is not expected to affect significantly the estimate[1].

[1]Considering PbLi isothermal at $T_{\text{Max}} = 823$ K, pressure loss would be around 5% lower than the current figure

Table 2: Connection pipe dimension at T_{ref}, according to Eq. (2), expressed in mm

Nominal diam.	Outer diam.	Inner diam.	Wall thickness
80	88.9	78.9	5
100	114.3	101.7	6.3
125	139.7	123.7	8
150	168.3	148.3	10
200	219.1	194.1	12.5
250	273	241	16
300	323.9	288.9	17.5

Fixed flow rate equal to $\Gamma_{\mathrm{IB}} = 5.32$ and $\Gamma_{\mathrm{OB}} = 16.38$ kg s^{-1} is assumed at the model/PbLi loop interface. Connection pipe sizing is defined according to

$$t_{\mathrm{w}} = \frac{D_{\mathrm{o}}(P + P_{\mathrm{h}})}{2[S_{\mathrm{a}} + 0.4(P + P_{\mathrm{h}})]} \tag{2}$$

where t_{w} is the wall thickness, D_{o} is the outer diameter (ranging from nominal diameter 80 to 300 mm), $P = 17.5$ MPa is the design pressure, $P_{\mathrm{h}} = 3$ MPa is the hydro-static load, and S_{a} is the maximum allowable stress (equal to 187 MPa at T_{ref}) [2]. Input values derived from Eq. (2) are collected in Table 2.

Enhanced pressure losses in the MHD regime are caused by Lorentz forces that oppose the flow bulk movement. Considering the steady momentum equation for an incompressible Newtonian fluid where the self-induced magnetic field is negligible [10]

$$(\mathbf{u} \cdot \nabla)\mathbf{u} = -\frac{1}{\rho}\nabla p + \nu\nabla^2\mathbf{u} + \frac{1}{\rho}\mathbf{J} \times \mathbf{B} \tag{3}$$

where $\mathbf{u}$, $\mathbf{J}$, ρ, and ν stands for velocity, current density, density, and kinematic viscosity.

For high magnetic field intensity, Eq. (3) is reduced in the bulk of the flow to a balance between pressure gradient and Lorentz force, therefore, it is possible to write for a fully developed flow in an electrically conductive duct

$$-\frac{\partial p}{\partial x} = k_{\mathrm{p}}\sigma u_0 B_0^2 \tag{4}$$

where u_0, B_0, σ, k_{p} stands for characteristic velocity, field intensity, fluid electrical conductivity, and pressure coefficient. This last quantity is determined by the wall conductance ratio $c = \sigma_{\mathrm{w}} t_w/\sigma a$, where σ_{w} and a stands for wall conductivity and characteristic length, i.e. half-width of the channel in the magnetic field direction or radius. The pressure coefficient is affected by duct geometry and electric boundary conditions [7, 11]. For uniform wall thickness, $k_{\mathrm{p}} = c/(1 + c)$ in a circular pipe and $k_{\mathrm{p}} = c/(1 + a/3b + c)$ for a rectangular duct with aspect ratio a/b. Similar relations are used for ducts with non-uniform wall thickness [7, 11].

The 2D (or baseline) MHD pressure drop that is caused by currents which are confined to the duct cross-section, a condition typical of fully developed flow, is estimated from Eq. (4). Whenever axial velocity gradients are present (e.g bends, cross-section variation, non-uniform magnetic field, etc.) additional currents are induced and cause further pressure loss. This quantity, called 3D loss, can be estimated with the relation

$$\Delta p_{3\mathrm{D}} = \frac{1}{2} k_{3\mathrm{D}} \rho u_0^2 N \tag{5}$$

with $k_{3\mathrm{D}}$ standing for the 3D pressure coefficient, which ranges in this study from 0.05 to 0.5 depending on the hydraulic element geometry, and $N = \sigma B_0^2 a/\rho u_0$ for the local interaction parameter [1].

For slowly spatially varying magnetic field and cross section, the flow is assumed to be locally fully developed and the pressure loss is calculated from the integral of Eq. (4), where u_0 and B_0 become a function of the axial coordinate [11]. This condition does not hold for the fringing field and, for this particular case, loss is estimate taking the maximum magnetic field value. Under these assumptions, MHD pressure loss is reduced in the present model to the sum of the integral of Eq. (4) and Eq. (5). Contributions from inertial, viscous, and electromagnetic coupling effects, although significant, are expected to be of second order importance for the blanket loss. They are partially accounted for in this study, to the extent that k_p and $k_{3\mathrm{D}}$ are derived by experimental studies and direct numerical simulations, but they still constitute a source of uncertainty that affects the estimate [7].

An "official" maximum allowable pressure loss (P_{max}) in the PbLi loop has not yet been defined in the EUROfusion project but it is reasonable for it to be significantly lower than P for safety reasons. In the following, we assume $P_{\mathrm{max}} = 5$ MPa as the theoretical upper limit for MHD pressure losses in the loop, allowing that the actual limit could be lowered by the maximum head available from the pumping system and plant economy considerations.

4. Connection pipes

In this region, a large contribution to the overall MHD loss is expected due to pipe length, large velocity, and high magnetic field. Three-dimensional loss from bends and cross-section variation have been shown by previous results to be negligible in this region compared with baseline pressure drop, calculated from Eq. (4), and, thus, are neglected [7]. The analysis has mostly been focused on IB, whereas OB model has been updated to reflect design changes since the previous study.

4.1. Outboard connection pipes

OB pipe routing has been designed to allow feeding from VV lower port and unloading from upper port to simplify blanket breeder path. The reference configuration foresees DN200 for both FP and DP. Regarding the latter, all the DP coming from one OB sector (3 OB segments) are merged into a top collector (DN350) to minimize port encumbrance.

The DP is attached to ≈ 2/3 of the OB poloidal height and this could cause potential issues due to inefficient PbLi drainage and accumulation of He bubbles but this layout is currently preferred for reasons of integration with other DEMO systems and ease of remote maintenance [7].

Introduction of the top collector does not affect significantly the DP loss estimate since contribution outside of TFC accounts only for 4.6% of the total, which is evaluated at 375.5 kPa. If the top collector size is reduced to DN200, a 4% loss increase is observed, which hints to a possible further reduction of the port encumbrance by adopting a smaller pipe. Revised DP layout has increased length within TFC that, in turn, leads to larger losses compared with previous estimate, 253 kPa, from Ref. [7].

FP layout has been revised to improve VV lower port integration and to make possible the use of a DN200 pipe. However, the updated routing has moved the pipe very close to one of the PFC. This design change allows large poloidal field intensity on a significant FP section (≈3.5 meter) that, in turn, causes a rise in the loss estimate from 354 kPa to 613 kPa. Consequently, the head loss caused by the poloidal field contribution rises as well from 20% to nearly 45% [7].

4.2. Inboard connection pipes

IB pipe routing follows the same general scheme described for OB. Reference dimensions are DN125 (FP) and DN150 (DP). A DN200 top collector is used to merge IB sector DPs and reduce port encumbrance.

FP path is adjacent to the VV port lower end and, consequently, is subjected to weaker poloidal field compared with OB (1.26 versus 2.96 T) but, conversely, features more than double the span within the TFC (≈6.6 versus ≈3 m) where the magnetic field reaches up to 8.64 T. IB FP smaller cross-section negates the advantage of lower flow rate compared with the OB FP and, therefore, mean velocity in the two components has roughly the same value. MHD pressure loss is estimated at 1557 kPa, which is nearly three times the OB FP figure. Only 4.3% of the loss is localized outside the TFC boundary. Ideally, the pressure loss across the FP should be no higher than 1000 kPa to keep the overall loss below $P_{\max} = 2000$ kPa. Mitigation strategies proposed are FP enlargement and insulation.

A larger pipe decreases mean velocity and, thus, losses, even if reduction is not linear as it would be expected from Eq. (4) due to the influence of wall thickness. At DN200, the IB FP loss approaches the figure calculated for OB (≈630 kPa) and then falls down it for DN>200 pipes that, however, are currently not consistent with remote maintenance requirements. Even if attractive, this solution will require a revision of the divertor/blanket integration layout and it may prove to be impractical.

Flow channel inserts (FCI) have shown promise in curtailing MHD losses in straight ducts through electrical decoupling of fluid and wall [7, 13]. Effect of insulation for continuous and discontinuous FCI on the reference IB FP loss is shown in Fig. 2. To model the effect of 3D losses at insulation gaps, the experimental results by Bühler et al. [13] have been extrapolated as described in Ref. [7]. Perfect insulation, either complete or limited to the TFC section, is very effective in reducing the loss, which falls below 400 kPa when 100% of the FP surface within the TFC is insulated. Manufacturing technology limits insert length at L=0.5 m, for which the estimated loss reaches up to 530 kPa, even if only 4% of the pipe surface is not insulated. If $L < 0.5$m, the insulation efficiency deteriorates rapidly and, as shown in Fig. 2, the pressure loss is equal to two-third of the naked pipe figure for $L = 0.1$m, which is still corresponds to a high percentage (80%) of the FP surface being insulated.

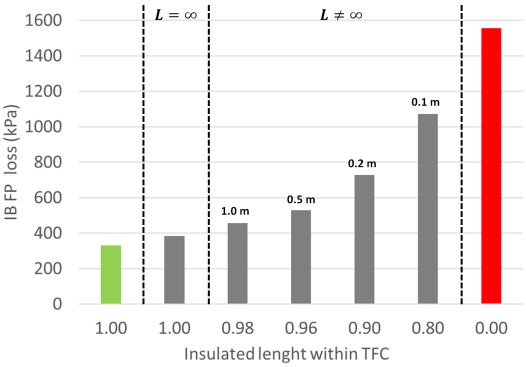

Figure 2: Effect of partial and continuous insulation on IB FP loss. Leftmost bar refers to complete insulation, whereas rightmost to naked pipe, i.e. no insulation. Insulated length within TFC is defined as nL/L_{TFC} with n number of inserts of length L and L_{TFC} pipe length within TFC inner surface.

The IB DP layout shows a similar trend to the OB and, for the reference configuration, loss is estimated at 260 kPa, of which only 12.1% is outside TFC. As discussed for the FP, pressure can be reduced by about 50%, i.e. to 153 kPa, by adopting a DN200 pipe in lieu of the one currently foreseen. Integration issues are less constraining in the upper port and this could be a viable option for the DP.

5. Spinal manifold

This hydraulic region has seen an important overhaul in the last design revision with the adoption of co-axial channels in lieu of stacked rectangular duct arrays, cfr. configuration T01.A in Ref. [7], to rationalize the manifold design and reduce losses. Detailed CFD analyses have been performed to investigate the MHD flow for the basic annular geometry [14] and coupled co-axial channel [15].

To estimate the manifold loss, the external (annular) duct is reduced to an equivalent rectangular channel (characterized by the same characteristic length, imposed mass flow rate, aspect ratio, and wall conductivity), for which Eq. (4) can be used to calculate a first-guess pressure gradient (∇p^*_{E}). This quantity is successively modified through multiplicative correction factors to account for the effect of annular geometry (ϵ_{E}) and coupling ($\epsilon_{\mathrm{E,c}}$). Similarly, a

correction factor is defined for the effect of coupling in the inner channel ($\epsilon_{\mathrm{I,c}}$), which pressure gradient is directly calculated from Eq. (4). These coefficient have been derived from the results of numerical simulations described in Refs. [14, 15].

5.1. Outboard spinal manifold

Mass flow rate and magnetic field intensity are spatially varying along the manifold length and the same is true for the pressure gradient calculated from Eq. (4),the evolution of which is shown in Fig. 3, where the abscissa is the breeding zone cell number (n). This phenomenon implies that the pressure loss for the arbitrary breeding zone cell depends on its position along the blanket spine determined with the linear spinal coordinate (s). If $\nabla p_{\mathrm{E}}(s) = \epsilon_{\mathrm{E}} \nabla p^*_{\mathrm{E}}$ and $\nabla p_{\mathrm{I}}(s) = \epsilon_{\mathrm{I}} \nabla p^*_{\mathrm{I}}$ are the corrected pressure gradients for, respectively, the external and internal channel, the manifold loss for the breeding zone cell at a certain position $s = s^*$ is expressed with the relation

$$\Delta p(s^*) = \int_0^{s*} \nabla p_E(s) \cdot \mathrm{d}s + \int_{s*}^{s_{\max}} \nabla p_I(s) \cdot \mathrm{d}s \qquad (6)$$

where $s = s_{\max}$ corresponds to the manifold upper end. In Fig. 4, the pressure loss estimated from Eq. (6) is presented for three scenarios, each one assuming different corrective factors, as a function of the breeding zone cell number. For the first scenario, only the external gradient is modified to account for annular geometry ($\epsilon_{\mathrm{E}} = 1.12$), whereas in the second one both channel gradients are corrected to represent the effect of mutual coupling ($\epsilon_{\mathrm{E,c}} = 1.59$, $\epsilon_{\mathrm{I,c}} = 2.41$). Lastly, the external channel factor is taken equal as the internal one to simulate the presence of obstacles (coolant pipes, breeding zone outlet, etc.) in this channel, which will cause additional 3D losses.

Coupling appears to be a very important phenomenon in the spinal manifold, nearly doubling the loss between the first (no coupling) scenario and the other cases for the OB manifold. Maximum loss including coupling is estimated from 236.5 to 257.8 kPa, about 50% less than the previous estimate ($\approx$ 458 kPa) that, however, neglected coupling effects [7]. This improvement is completely ascribable to the revised spinal manifold configuration, which features larger cross-section compared with the one considered in Ref. [7]. The pressure imbalance ratio between the blanket cell with maximum ($\Delta p_{\max}$) and minimum loss ($\Delta p_{\min}$) for the coupled scenario is quite significant at $\Delta p_{\max}/\Delta p_{\min} = 3.07$. Since cells at the OB top ($n > 80$) are characterized by low head losses, as shown in Fig. 4, it is reasonable to expect severe overfeeding for cells there.

5.2. Inboard spinal manifold

The smaller toroidal width of the IB influences the manifold geometry, which is composed by a narrower external channel and, therefore, a higher blockage ratio ($\beta_{\mathrm{IB}} = A_{\mathrm{i}}/A_{\mathrm{e}} = 0.56$ versus $\beta_{\mathrm{OB}} = 0.34$, where A_{i} and A_{e} are the internal and external channel area). Corrective

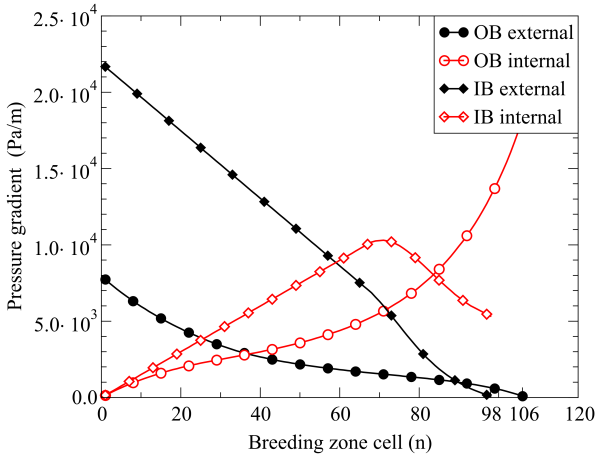

Figure 3: Spinal manifold pressure gradient for OB and IB, without corrective factor ϵ_i. Maximum cell number ($n_{\max}$) is 98 and 106 for IB and OB

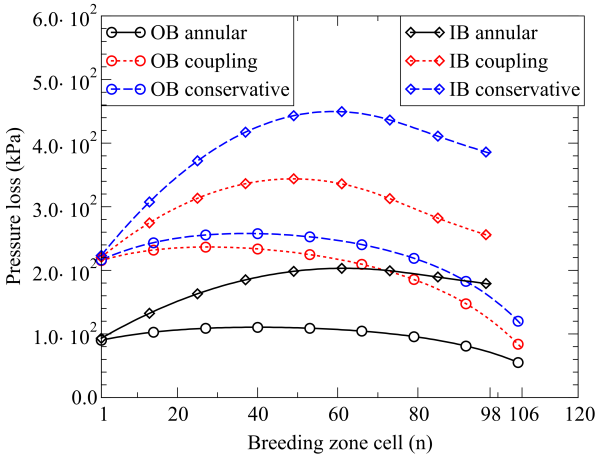

Figure 4: Spinal manifold loss for IB and OB. Three scenarios are assumed to assess the effect of coupling and manifold channel complex geometry: annular ($\epsilon_{\mathrm{E}} = 1.12$, $\epsilon_{\mathrm{I}} = 1$), coupling ($\epsilon_{\mathrm{E,c}} = 1.59$, $\epsilon_{\mathrm{I,c}} = 2.41$), and conservative ($\epsilon_{\mathrm{E,c}} = 2.41$, $\epsilon_{\mathrm{I,c}} = 2.41$).

factors determined from OB geometry are used to calculate losses in this configuration but are likely to require revision in the future since, even if ϵ_{E} does not appear to depend on the magnetic field intensity at IB values [14, 15], it is expected to be blockage ratio sensitive. The same scenarios described for the OB are used to assess the IB manifold loss under different assumptions.

Manifold pressure gradient and loss for the arbitrary inboard cell are presented in Fig. 3 and Fig. 4. Conversely to the OB, it is the external annular channel that contributes more, since it is characterized by higher mass flow rate at the blanket bottom where the maximum toroidal field is localized. The top IB section is subjected to a quick field decrease and, as a result, the internal channel gradient falls below its maximum point even though the flow rate is still increasing.

Maximum cell loss is estimated from Eq. (6) between

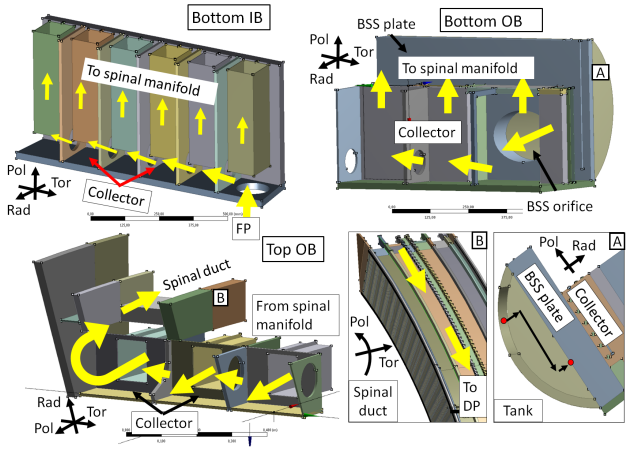

Figure 5: WCLL IB/OB terminal collectors. Top: bottom IB and OB assembly (for which the internal channels of the spinal manifold are omitted for clarity). Bottom: top main collector, detail of flow in the top OB collector spinal duct and bottom OB intermediate tank

343.7 to 449.6 kPa under scenario two and three, where the latter value accounts for uncertainties and obstacle presence. The estimate is partially penalized by channels aligned with radial direction; a possible IB design revision could address this point by adopting slender channels in the toroidal direction. The cell with the maximum loss is located more toward the equatorial plane compared with OB and, as a result, the pressure imbalance ratio is equal to just 1.51 for the coupled scenario and overfeeding is expected for cells at both blanket extremities.

6. Terminal collectors

The terminal collectors are integrated with the spinal manifold and constitute its lower and upper extremities bridging the gap with the connection pipes. This hydraulic region is the most complex from a geometrical perspective and is where 3D currents and other second order effects are expected to contribute more for MHD loss and flow distribution. Consequently, itwould also benefit the most from detailed 3D analyses to reduce the estimate uncertainty.

6.1. Outboard terminal collectors

The OB terminal collector region is divided into two main areas: the bottom and top assemblies which are dedicated, respectively, to PbLi feeding and collecting functions.

In the bottom assembly, an intermediate tank welded at the BSS receives PbLi from the OB FP and conveys it toward the collector, corresponding to the spinal manifold lower end. In Fig. 5 (bottom OB), the geometry and main hydraulic elements of the OB bottom assembly are shown. Head loss estimate is detailed in Table 3, where intermediate tank and MHD flow through BSS are the main contributor.

Tank pressure loss estimate is likely affected by a significant uncertainty since the problem is hardly similar to MHD duct flow, from which both Eqs. (4) and (5) are derived. Passage through thick BSS is responsible for nearly a third of the overall loss, even though it constitutes a tiny fraction of the hydraulic path. The collector channels are connected through SP orifices, but do not appear to exhibit strong pressure imbalance. Flow distribution will more likely be determined by coupling phenomena in this region.

Similarly, the top main collector constitutes the spinal manifold final part and its main task is to convey PbLi toward the spinal duct, embedded within BSS, and the DP attachment point. The BSS duct is the main loss contribution due to its length and contact with thick structural elements. The main collector shows relatively high losses compared with the bottom assembly, despite their similarity, due to the sudden cross-section variation at the interface with the spinal duct. Attachment to the DP is ensured by BSS orifices and secondary pipes. Passage through the BSS and merging into the main DP are responsible for the bulk of pressure losses in this hydraulic element.

6.2. Inboard terminal collectors

The bottom and top IB assemblies have a more straightforward geometry compared with the OB system and are, strictly speaking, extrapolated from the OB geometry. The breeder enters the IB bottom assembly through an orifice drilled in the bottom cap plate, as it is shown in Fig. 5, which connects the IB with the FP avoiding to pass through the thicker BSS, as it is instead the case for the OB collector. The top IB assembly is very similar to the OB one with the difference that the DP is directly attached to the IB topmost point, which allows easier draining without the need for a spinal duct.

Although exposed to generally higher field intensity, IB collectors feature lower losses compared with OB thanks to the more streamlined layout. Flow through thick plates is a dominant contribution to the overall estimate (41% and 55% for the bottom and top collectors, respectively). Regarding flow distribution, no significant pressure imbalance was observed across flow paths and, therefore, coupling is expected to dominate this aspect.

7. Conclusions

An overview of the overall MHD loss in the PbLi loop feeding one IB and OB segment is presented in Table 3, broken down by hydraulic region, for the most recent WCLL design iteration. The largest contribution is made by the piping system, equal to about 62% and 75% for OB and IB respectively. The terminal collectors account for a larger loss share (23%) in OB due to a more complex layout, namely the BSS duct required to connect the top collector and DP attachment. The spinal manifold is the second largest contribution in the IB (19%).

As expected, the total MHD loss estimate is lower than $P_{\max}$ for both IB and OB loops. Following the outcome of

Table 3: MHD loss in WCLL IB and OB expressed in MPa, percentage contribution by hydraulic region in brackets

	Inboard		Outboard	
Feeding pipe	1.557	(63.9)	0.613	(38.1)
• Inside TFC	1.489		0.338	
• Outside TFC	0.067		0.276	
Terminal collector/Bot	0.092	(3.8)	0.122	(7.6)
• Collector			0.013	
• Intermediate tank			0.065	
• BSS orifice			0.044	
Spinal manifold	0.450	(18.5)	0.258	(16.0)
• External ch.	0.328		0.068	
• Internal ch.	0.122		0.190	
Breeding zone	negligible		negligible	
Terminal collector/Top	0.076	(3.1)	0.241	(15.0)
• Collector			0.055	
• BSS duct			0.123	
• DP attachment			0.063	
Draining pipe	0.260	(10.7)	0.376	(23.4)
• Inside TFC	0.229		0.358	
• Outside TFC	0.031		0.017	
Total	2.435	(100 %)	1.609	(100 %)

this analysis, the pumping system design has been revised to achieve a nominal pressure head $H_{\mathrm{OB}} = 15$ m and $H_{\mathrm{IB}} = 30$ m for the required blanket flow rate. A more realistic maximum acceptable MHD loss has then been derived from the maximum achievable head: $P_{\mathrm{max,OB}} = 2$ MPa and $P_{\mathrm{max,IB}} = 3$ MPa. Further optimization of the PbLi loop design should be aimed to reduce pressure losses to improve the plant economy and achieve a good flow distribution.

Regarding loss minimization, it is considered too challenging to revise the connection pipe layout due to the numerous plant constraints on it. The introduction of FCI could be a viable mitigation strategy and it should be carefully considered, in particular for the IB loop, since it shows significant potential, even if some open issues still remain for a successful implementation. On the other hand, the internal blanket geometry is subjected to less plant constraints and the manifold layout (both collector and spinal) is going to be revised to improve its performances in the next WCLL iteration.

Experimental work on collector mock-ups and 3D numerical simulations are strongly desirable to reduce the uncertainty on the total pressure loss estimate and give some insights on the PbLi flow distribution in the blanket; an aspect that, although important for tritium inventory control, has not yet been studied in detail. Future analyses will aim to improve and expand upon the current estimate by removing the simplifying assumptions of isothermal flow and uniform flow distribution in the blanket.

Acknowledgements

This work has been carried out within the framework of the EUROfusion Consortium and has received funding from the Euratom research and training programme 2014-2018 and 2019-2020 under grant agreement No 633053. The views and opinions expressed herein do not necessarily reflect those of the European Commission.

References

[1] S. Smolentsev, R. Moreau, L. Bühler, C. Mistrangelo, MHD thermofluid issues of liquid-metal blankets: phenomena and advances, Fusion Engineering and Design 85 (2010) 1196–1205. Doi: 10.1016/j.fusengdes.2010.02.038.

[2] A. Del Nevo, P. Arena, G. Caruso, P. Chiovaro, P. Di Maio, M. Eboli, F. Edemetti, N. Forgione, R. Forte, A. Froio, et al., Recent progress in developing a feasible and integrated conceptual design of the WCLL BB in EUROfusion project, Fusion Engineering and Design (2019). Doi: 10.1016/j.fusengdes.2019.03.040.

[3] M. Utili, S. Bassini, L. Boccaccini, L. Bühler, F. Cismondi, A. Del Nevo, M. Eboli, F. Di Fonzo, T. Hernandez, S. Wulf, et al., Status of Pb-16Li technologies for European DEMO fusion reactor, Fusion Engineering and Design (2019). Doi: 10.1016/j.fusengdes.2019.04.083.

[4] J. Reimann, et al., Report of the Working Group MHD for the Blanket Concept Selection Exercise (BCSE, Forschungszentrum Karlsruhe, 1995. Tech. Rep. FZKA 5652.

[5] D. Rapisarda, I. Palermo, M. Gonzalez, F. Martin-Fuertes, C. Moreno, A. Ibarra, I. Fernandez, E. M. de les Valls, Overview of DCLL research activities in the EU/Spain, in: 2015 IEEE 26th Symposium on Fusion Engineering (SOFE), IEEE, 2015, pp. 1–8. Doi: 10.1109/SOFE.2015.7482358.

[6] P. Swain, P. Koli, S. Ghorui, P. Mukherjee, A. Deshpande, Thermofluid mhd studies in a model of indian llcb tbm at high magnetic field relevant to iter, Fusion Engineering and Design 150 (2020) 111374. Doi: 10.1016/j.fusengdes.2019.111374.

[7] A. Tassone, G. Caruso, A. Del Nevo, Influence of PbLi hydraulic path and integration layout on MHD pressure losses, Fusion Engineering and Design 155 (2020) 111517. Doi: 10.1016/j.fusengdes.2020.111517.

[8] D. Martelli, A. Venturini, M. Utili, Literature review of lead-lithium thermophysical properties, Fusion Engineering and Design 138 (2019) 183–195. Doi: 10.1016/j.fusengdes.2018.11.028.

[9] K. Mergia, N. Boukos, Structural, thermal, electrical and magnetic properties of Eurofer 97 steel, Journal of Nuclear Materials 373 (2008) 1–8. Doi: 10.1016/j.jnucmat.2007.03.267.

[10] U. Müller, L. Bühler, Magnetofluiddynamics in channels and containers, Springer Science & Business Media, 2013.

[11] I. R. Kirillov, C. B. Reed, L. Barleon, K. Miyazaki, Present understanding of MHD and heat transfer phenomena for liquid metal blankets, Fusion engineering and design 27 (1995) 553–569. Doi: 10.1016/0920-3796(95)90171-X.

[12] M. Abdou, N. B. Morley, S. Smolentsev, A. Ying, S. Malang, A. Rowcliffe, M. Ulrickson, Blanket/first wall challenges and required R&D on the pathway to DEMO, Fusion Engineering and Design 100 (2015) 2–43. Doi: 10.1016/j.fusengdes.2015.07.021.

[13] L. Bühler, H.-J. Brinkmann, C. Koehly, Experimental study of liquid metal magnetohydrodynamic flows near gaps between flow channel inserts, Fusion Engineering and Design (2018). Doi: 10.1016/j.fusengdes.2018.11.034.

[14] S. Siriano, A. Tassone, G. Caruso, A. Del Nevo, MHD forced convection flow in dielectric and electro-conductive rectangular annuli, Fusion Engineering and Design (2020). Doi: 10.1016/j.fusengdes.2020.111773.

[15] S. Siriano, A. Tassone, G. Caruso, A. Del Nevo, Electromagnetic coupling phenomena in co-axial rectangular channels, Fusion Engineering and Design (2020). ISFNT-14 (This conference, in press).